

Article

# Incremental Forming of Titanium Ti6Al4V Alloy for Cranioplasty Plates—Decision-Making Process and Technological Approaches

Sever Gabriel Racz, Radu Eugen Breaz \* , Melania Tera , Claudia Gîrjob, Cristina Biriş, Anca Lucia Chicea and Octavian Bologna

Department of Industrial Machines and Equipment, Engineering Faculty, “Lucian Blaga” University of Sibiu, Victoriei 10, 550024 Sibiu, Romania; gabriel.racz@ulbsibiu.ro (S.G.R.); melania.tera@ulbsibiu.ro (M.T.); claudia.girjob@ulbsibiu.ro (C.G.); cristina.biris@ulbsibiu.ro (C.B.); anca.chicea@ulbsibiu.ro (A.L.C.); octavian.bologa@ulbsibiu.ro (O.B.);

\* Correspondence: radu.breaz@ulbsibiu.ro; Tel.: +40-745-374-776

Received: 4 July 2018; Accepted: 6 August 2018; Published: 9 August 2018



**Abstract:** Ti6Al4V titanium alloy is considered a biocompatible material, suitable to be used for manufacturing medical devices, particularly cranioplasty plates. Several methods for processing titanium alloys are reported in the literature, each one presenting both advantages and drawbacks. A decision-making method based upon AHP (analytic hierarchy process) was used in this paper for choosing the most recommended manufacturing process among some alternatives. The result of AHP indicated that single-point incremental forming (SPIF) at room temperature could be considered the best approach when manufacturing medical devices. However, Ti6Al4V titanium alloy is known as a low-plasticity material when subjected to plastic deformation at room temperature, so special measures had to be taken. The experimental results of processing parts from Ti6Al4V titanium alloy by means of SPIF and technological aspects are considered.

**Keywords:** single-point incremental forming; AHP; cranioplasty plates; decision-making; titanium alloys; medical devices

## 1. Introduction

Titanium alloys are considered eligible materials for biomedical applications (implants and prosthetic devices) due to their biocompatibility. The work presented in [1] provides a comprehensive analysis regarding the main types of titanium alloys used in biomedical applications, as well as their advantages and main drawbacks. A review regarding the titanium alloys seen as the best solution for orthopedic implants is presented in [2], where also the main requirements for a material to be considered a biomaterial are introduced. One of the requirements for this is biocompatibility, which according to [3] is measured by how the human body reacts to the device made of this material when it is implanted. In this work, hip and knee implants are defined as the main orthopedic implants. Both studies presented in [1] and [2] mention Ti6Al4V alloy as one of the titanium alloys; it was initially developed for the aeronautical industry, but can be successfully used for biomedical applications.

Cranioplasty is another main field where titanium alloys may be used due to their biocompatibility. A detailed review about the techniques and materials used in cranioplasty is presented in [4]. Titanium is considered one of the suitable materials, being biocompatible but hard to shape. Another review [5] also indicated titanium alloys as one the materials of choice for cranioplasty plates.

The work presented in [6] reported the successful use of 300 plates of titanium for cranioplasty. The requested shape of the cranioplasty plate was determined either by a traditional technique or

by means of computer tomographic scans. Finally, the plates were shaped by pressing them against a counter-die, which could be considered a plastic deformation process. A comprehensive study presented in [7] confirmed titanium alloys as one of the recommended materials for cranioplasty plates, but also highlighted the fact that complications occurred in 29% out of 127 cases. However, the recommendations were to strengthen the prophylaxis measures against infections, rather than replacing titanium as the material for cranioplasty plates. The research was not focused upon the method of manufacturing titanium cranioplasty plates.

Another study reporting the use of titanium plates for cranioplasty was presented in [8]. The work was towards using CAD (computer aided design)/CAM (computer aided manufacturing) methods for manufacturing the plates. A rapid prototyping method based upon fine casting was used and it was reported as having several advantages compared with a traditional milling process.

Titanium alloys were considered the best choice for cranioplasty of large skull defects, according to the results presented in [9]. The study was based upon long-term observations of 26 patients and emphasized the fact that none of the titanium plates implanted had to be removed. Even if the study mentioned CAD/CAM techniques for manufacturing cranioplasty plates, these techniques were not described in detail, and were mostly oriented on the generation of the requested shape of the plate using computer tomography, rather than presenting how the plates were manufactured.

The approaches regarding the methods of manufacturing the titanium plates for cranioplasty are very diversified. The study presented in [10] emphasized the advantages of a manual approach (the shape of the plate was obtained by pressing the titanium sheet against a template model using a manual press), while in [11] the shape of the plate was obtained by means of multiforming, a method which requires very complex technological equipment with a high degree of automatization.

Thus, it can be concluded that titanium alloys are suited for manufacturing cranioplasty plates and there is no consecrated technological approach, either manual or automated, for that. Finding a suitable method for manufacturing the plates was one of the objectives of this work and it involves, in the first stage, a review of the main methods of manufacturing parts from titanium alloys.

The work presented in [12] emphasizes the effects of machining Ti6Al4V alloy by means of cutting, using tools made of straight-grade cemented carbide. Microstructure alterations were reported and, moreover, the reported surface roughness falls into the rough machining category. Consequently, cutting processes may not be the recommended solution when machining biomedical devices from titanium alloys.

Usually, the titanium alloys are also low-plasticity materials, so processing them by means of plastic deformation is also difficult. Single-point incremental forming (SPIF) is one of the manufacturing processes used for processing titanium alloys to overcome the drawback introduced by the low plasticity of these materials, which prevents their processing by other plastic deformation processes. A schematic diagram of the SPIF process is presented in Figure 1, where the sheet metal workpiece (2) is fixed by means of the retaining plate (3) and active plate (backing plate) (1). The punch (4) is moving in the vertical direction, along the Z axis, while the assembly formed by (1)–(3) executes a movement in the XY plane. By combining these movements, various trajectories can be achieved and, subsequently, different shapes of the sheet metal final part.

Literature reviews regarding the SPIF process are presented in [13], which covers the results obtained before 2005, and most recently in [14], which synthesizes the research results reported between 2005 and 2015. The influence of various SPIF process parameters upon the results is synthesized in [15]. It is here noticeable the fact that the maximum achievable angle for a truncated cone part made of Ti6Al4V alloy processed by SPIF using a 10 mm diameter punch reported in [14] was 32°, the lowest one compared with all materials processed by means of SPIF. For comparison, for similar geometry and tool but for DC04 steel and AA 5754 (AlMg3) aluminum alloy, the reported maximum wall angles were 64° and 71°, respectively. These results stress the fact that special measures must be taken when unfolding the SPIF process using titanium alloys as workpieces.



by SPIF was presented in [25], where friction obtained by tool rotation was used. At speeds between 2000 and 7000 rpm, the heat generated by friction improved the formability of the parts, but as pointed out by the authors it is not only due to material softening, but also to recrystallization. However, the material used for this research was AA5052-H32 aluminum alloy, so no information about using frictional heat for machining titanium alloys by means of SPIF was available.

A master–slave tool layout for double-side incremental forming (DSIF) combined with electrically assisted heating was presented in [26]. Good results were reported in processing lightweight materials (AZ31B magnesium alloy) with regards to surface quality and maximum wall angle for truncated cone parts and a new type of hybrid toolpath lead to better geometric accuracy. However, the machining layout for DSIF, which must be custom-built, and the necessity to control and synchronize the toolpaths of the master and slave tools could lead to very high machining costs in contrast to the real value of the machined parts.

With regards to the influence of high temperatures applied during manufacture processes upon the biocompatibility of titanium alloys, there are still many opinions. The biocompatibility of these materials is related to the spontaneous formation of a passive oxide layer at room temperature, which is reported to reduce oxygen diffusion and further oxidation at lower temperatures [27–29]. However, at higher temperatures the situation is changing. The works presented in [30–32] consider that oxidation at high temperatures limits the applications of these kind of alloys. In [30] is stated the fact that diffusion of oxygen at temperatures above 400 °C leads to the development of a hard and brittle oxygen diffusion zone which leads to a loss of tensile ductility and of fatigue resistance, reducing the life expectancy of titanium alloys. Above 600 °C, a thick and defective oxide layer is formed, facilitating the penetration of oxygen into the material [30]. Aluminum was found to diffuse outwards through the oxide layer in the later oxidation stage [33]. A study reported in [29] stated that the presence of aluminum in outer layers of Ti6Al4V alloy may hinder osteointegration (bone bonding to the implant) when used as an implant material. Also, aluminum is known to cause neurological disorders [34].

However, a controlled oxidation process called “thermal oxidation” at high temperature is also seen as a promising technique to improve protection against friction and wear [30,32,35–37].

There are also arguments which support the fact that forming titanium alloys at high temperature does not affect their compatibility. Promising results regarding the manufacturing of cranioplasty plates by SPIF with material heating were presented in [38]. The workpiece was heated at 650 °C during the SPIF process and impact tests were performed to measure the maximum force and energy absorbed by the plate. Furthermore, a cytotoxicity test was also performed to assess if the manufacturing process affected the biocompatibility of the plate. The test showed no differences between the processed surfaces and the control ones with regards to biocompatibility. The work presented in [39] had shown that the influence of oxygen enrichment during the process of manufacturing cranial prostheses by means of superplastic forming did not affect the biocompatibility of the Ti6Al4V alloy. A cytotoxicity test was performed, and the viability of the cells was not affected.

Consequently, it is not yet fully demonstrated if heating the material during the process does or does not affect its biocompatibility. However, processing at high temperatures significantly improves the plasticity of the titanium alloys. On the other hand, the complexity of the equipment, the costs associated with that complexity (and with higher energy consumption), and the difficulty of controlling the process favor processing at room temperature, if plasticity requirements can be fulfilled.

From an environmental and sustainability point of view, recent works have pointed out that SPIF is a process with higher amounts of energy consumption compared with other forming processes, such as stamping [40]. The studies presented in [41] have indicated tool speed, type of material, and vertical incremental step in this order as the main influence factors upon the amount of energy consumption during the SPIF process. A similar study which also took into consideration the technological equipment (CNC machine, six-axes industrial robot, and dedicated Amino machine) was presented in [42] and emphasized the fact that forming time is the most influential factor upon the

electric energy consumption. Based upon this assumption, the study presented in [43] compared the energy efficiency of performing SPIF machining on a CNC milling machine and on a high-speed CNC lathe. The results have demonstrated that high-speed processing significantly reduces the processing time and, consequently, the energy consumption. Environmental aspects must be considered every time machining is involved, but medical devices such as implants and prosthetic devices are usually machined as prototypes; thus, the environmental impact manufacturing them should be considered quite low. However, reducing the overall machining time is one of the most recommended approaches from this point of view.

The authors of this work have performed some previous studies with regards to using complex trajectories and computer-assisted techniques in SPIF processes [44,45] and some preliminary work in the field of using titanium alloys in cranial implants [46].

As presented above, there are many techniques in use for manufacturing cranioplasty plates from Ti6Al4V alloy, each one with advantages and drawbacks. However, as presented in the next section, single-point incremental forming at room temperature could be considered the best choice, if some criteria are considered. Of course, as reported in the literature, the low plasticity of the Ti6Al4V alloy makes it difficult to process it in this condition. Thus, the approach presented in this paper was oriented towards finding some technological approaches which could allow for better processing of Ti6Al4V alloy at room temperature. As results, some incremental findings, linked mainly with the types of toolpaths and the values of processing steps, with regards to the proposed objective were synthesized.

## 2. Materials and Methods

### 2.1. Decision-Making Process

Cranioplasty plates may be manufactured using either a manual or a digital approach (Figure 2). The input data come either from a physical template (a bone fragment taken from the patient) or from a computer tomography (CT) scan. If the manual manufacturing approach is chosen, by means of the physical template, a negative cast is made using laboratory putty. The following steps involve several manual operations, which may differ from one method to another. A comprehensive description of a manual method for manufacturing cranioplasty plates is presented in [10].

The digital approach relies heavily on CAD (computer-aided design)/CAM (computer-aided manufacturing) techniques. The data from the CT scan is processed and converted from a point cloud model to a 3D STL (stereolithography) file format by means of any CAD software package. The 3D model is imported into any CAM software where processing technology and machining code are generated and sent to the technological equipment (CNC machine tool, industrial robot, or even a specialized machine). The format of the machining code and the type of the technological equipment depend on the technological process used for the actual manufacturing of the cranioplasty plate. No matter the chosen manufacturing method, in the final stage, the cranioplasty plate is subjected to some specific operations to prepare it for implantation (i.e., sterilization).

According to the literature review presented above, the most recommended manufacturing processes for cranioplasty plates are cutting (CUT), single-point incremental forming (SPIF), single-point incremental forming with heating (SPIFH), and double-side incremental forming (DSIF). A special mention should be made with regards to additive manufacturing methods, which were recently reported as effective methods for manufacturing cranioplasty plates. An approach presented in [47] presented a two-stage method for manufacturing a cranioplasty plate. In the first stage, by means of 3D printing, a mold was manufactured which was further used for casting a polymethyl-methacrylate (PMMA) cranioplasty plate in the second stage. More recently, an industrial company presented a case study [48] in which a cranioplasty plate was manufactured using a metal 3D printing machine, using Ti MG1 (ISO 10993) as the material.

However, the current research is oriented upon using Ti6Al4V as the material for manufacturing a cranioplasty plate; thus, only CUT, SPIF, SPIFH, and DSIF will be considered for the analysis.

A decision-making method for selecting between these processes based upon AHP (analytic hierarchy process) was developed during this research.

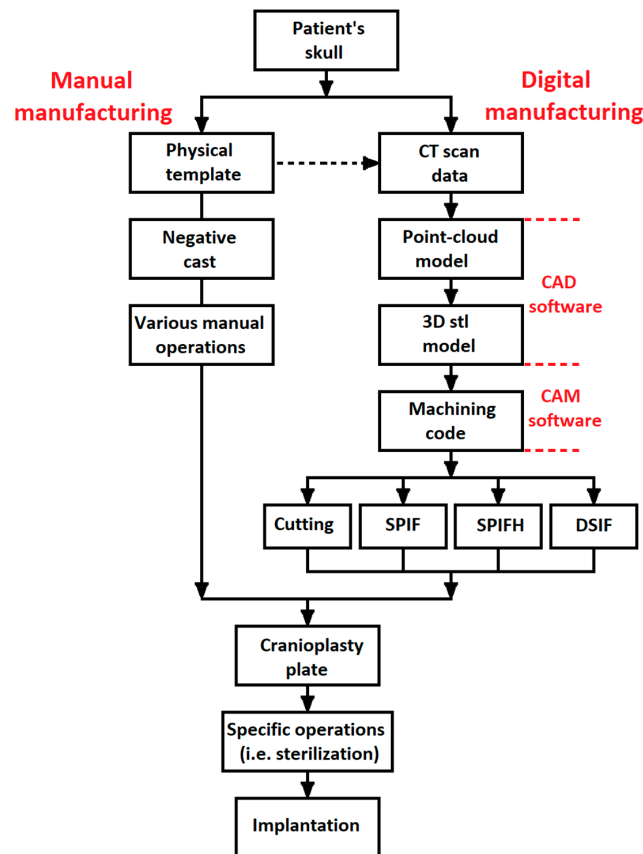


Figure 2. Manufacturing processes for cranioplasty plates.

Comparing the four considered manufacturing processes is a multiattribute decision-making problem due to the factors involved. One of the methods which can be used for this purpose is the Analytic Hierarchy Process (AHP), a method introduced by Saaty [49,50]. The method is based upon pairwise comparison. Elements  $i$  and  $j$  are compared, and the result is expressed by value  $a_{ij}$ . A given hierarchization criteria is used for the comparison:

$$a_{ij} = 1 \quad \text{for } i = j, \quad \text{where } i, j = 1, 2, \dots, n$$

$$a_{ij} = \frac{1}{a_{ji}} \quad \text{for } i \neq j \quad (1)$$

The judgement scale, used for AHP, was proposed by Saaty: 1, equally important; 3, weakly more important; 5, strongly more important; 7, demonstrably more important; 9, absolutely more important. The values in between (2, 4, 6, and 8) represent compromise judgements.

To use the AHP process for comparing the four manufacturing processes, a set of seven criteria were proposed and compared pairwise against each other. The preference matrix from Table 1 is used to store the results. The six proposed criteria are presented below:

- C1—Formability: seen here as the ability of the manufacturing process to modify the shape of the workpiece by redistributing the material (plastic deformation). It is noticeable here that three of the analyzed processes are plastic deformation processes, while one of them (CUT) is based upon

shaping the part by removing material. However, it was considered that this criterion could be also applied to the CUT process;

- C2—Microstructure: seen here as a measure of how the microstructure of the material is affected by the manufacturing process and, consequently, how the biocompatibility of the processed part could be affected;
- C3—Degree of control: seen here as a measure of how the parameters of the process and the shape and dimensional parameters of the parts (cranioplasty plates) can be controlled;
- C4—Roughness: the meaning of this criterion is quite straightforward, as it expresses the surface quality achievable for the processed parts;
- C5—Energy consumption: it is related with the amount of energy required by each manufacturing process;
- C6—Accuracy: seen here as the maximum achievable accuracy for the parts processed by each of the analyzed manufacturing processes;
- C7—Production time: seen here as the total amount of time to produce a cranioplasty plate.

**Table 1.** Preference matrix A.

Criterion	C1	C2	C3	C4	C5	C6	C7
C1	1	1/3	5	3	7	3	5
C2	3	1	9	3	9	5	3
C3	1/5	1/9	1	1/5	3	1/5	1/5
C4	1/3	1/3	5	1	7	5	1/3
C5	1/7	1/9	1/3	1/7	1	1/7	1/7
C6	1/3	1/5	1/5	1/5	7	1	1/3
C7	1/5	1/3	5	3	7	3	1

As an example, the way in which the first line of Table 1 was filled is presented below:

- Microstructure (C2) and formability (C1) are very important characteristics of a cranioplasty plate; however, for a device in contact with the human tissue, the state of the microstructure should be considered weakly more important than the ability of shaping the plate;
- The degree of control (C3) is a measure of the quality and repeatability of the process. A higher degree of control will allow the process to be automated, but, finally, for a prosthetic device (which can also be manufactured manually), the ability to shape the plate exactly as required (C1) is strongly more important;
- Roughness (C4) of the part is also important for a prosthetic device, but while the microstructure cannot be repaired if affected by the manufacturing process, roughness could be improved (even by manual operations); thus, the formability of the plate (C1) should be considered weakly more important;
- Energy consumption (C5) should be reduced as possible for any manufacturing process; however, when it comes to cranioplasty plates (which usually are manufactured as prototypes), the ability of shaping the part should (C1) be considered demonstrably more important than saving energy (C5);
- Manufacturing accuracy of the cranioplasty plate (C6) is important, but from the point of view of its functional role (prosthetic device, which is not moving or being in contact with other moving parts), the formability (C1) should be considered weakly more important;
- Production time (C7) is a measure of the efficiency of a production process, but taking into consideration of the fact that, as stated for the (C5) criterion, the cranioplasty plates are manufactured as prototypes, the (C1) criterion should be considered strongly more important.

The next step of the AHP process involves the normalization of the preference matrix by transforming it into matrix B, where

$$B = [b_{ij}] \quad (2)$$

$$b_{ij} = \frac{a_{ij}}{\sum_{i=1}^n a_{ij}}$$

It is now required to calculate the eigenvector  $w = [w_i]$ , which expresses the preference between the elements, by using the following relationship:

$$w_{ij} = \frac{\sum_{i=1}^n b_{ij}}{n} \quad (3)$$

The normalized B is presented in Table 2. The eigenvector w was placed on the last column of matrix B, calculated using Equation (3).

**Table 2.** Normalized matrix B.

Criterion	C1	C2	C3	C4	C5	C6	C7	w
C1	0.1996	0.1458	0.3024	0.3842	0.2188	0.2901	0.2239	0.2256
C2	0.5989	0.4375	0.4234	0.3842	0.2188	0.2901	0.3134	0.3905
C3	0.0399	0.0625	0.0605	0.0427	0.0938	0.0193	0.1343	0.0558
C4	0.0665	0.1458	0.1815	0.1281	0.2188	0.2901	0.1343	0.1777
C5	0.0285	0.0625	0.0202	0.0183	0.0313	0.0138	0.0149	0.0233
C6	0.0665	0.1458	0.0121	0.0427	0.2188	0.0967	0.1343	0.0829
C7	0.0384	0.0640	0.0160	0.0423	0.0811	0.0227	0.0448	0.0442

The comparisons must be checked from the point of view of consistency, according to [48–51]. The check is made by calculating the maximal eigenvalue according to

$$\lambda_{max} = \frac{1}{n} \sum_{i=1}^n \frac{(Aw)_i}{w_i} = 7.4469 \quad (4)$$

where  $\lambda_{max}$  is the matrix's largest eigenvalue [34].

Using the random consistency index table (Table 3) from [50], the consistency ratio CR may be determined (for a 6-dimensional matrix, the r coefficient is 1.32).

**Table 3.** Values for CI indices.

Size of Matrix (n)	1	2	3	4	5	6	7	8	9	10
Random average CI (r)	0	0	0.58	0.90	1.12	1.24	1.32	1.41	1.45	1.51

According to Equation (5), the value of CR is smaller than 10%, showing that the comparisons made during the building of matrices A and B are consistent [36,37].

$$CR = \frac{\lambda_{max} - n}{r(n-1)} = 5.64\% \quad (5)$$

The evaluation of the four manufacturing strategies with respect to the seven criteria will be unfolded below. The evaluation for each criterion is presented in Tables 4–10, together with the eigenvectors (introduced in the last column of each table). For exemplification, the way in which the second line of Table 4 was filled is presented below:

- Cranioplasty plates are manufactured starting from a sheet metal workpiece; thus, a plastic deformation process (SPIF) should be considered as an intermediate between equally important and weakly more important than a cutting process (CUT) from the point of view of formability (C1). Even the workpiece is different for cutting, and cutting also allows the user to machine complex shapes; thus an intermediate value has been considered;

- Ti6Al4V alloy is known as a low-formability material, and heating it leads to an increase in the formability. However, applying heat could lead to some problems described above. Thus, SPIFH should be considered weakly more important than SPIF, from the (C1) point of view;
- Using a master–slave tools layout with punch and counter-punch will significantly improve the formability of the part, but will also lead to the use of very complex layouts and equipment; this is why DSIF should be considered weakly more important than SPIF, from the (C1) point of view.

**Table 4.** Comparison of the processing strategies with regards to C1 (formability).

C1	CUT	SPIF	SPIFH	DSIF	w
CUT	1	1/2	1/2	1/2	0.1386
ASPIF	2	1	1/3	1/3	0.1622
ASPIFH	2	3	1	1/2	0.2902
DSPIF	2	2	2	1	0.4090

**Table 5.** Comparison of the processing strategies with regards to C2 (microstructure).

C2	CUT	SPIF	SPIFH	DSIF	w
CUT	1	1/9	1/5	1/7	0.0399
ASPIF	9	1	7	7	0.6440
ASPIFH	5	1/7	1	1/3	0.1145
DSPIF	7	1/7	3	1	0.2016

**Table 6.** Comparison of the processing strategies with regards to C3 (degree of control).

C3	CUT	SPIF	SPIFH	DSIF	w
CUT	1	3	5	5	0.5143
ASPIF	1/3	1	5	5	0.3045
ASPIFH	1/5	1/5	1	3	0.1158
DSPIF	1/5	1/5	1/3	1	0.0654

**Table 7.** Comparison of the processing strategies with regards to C4 (roughness).

C4	CUT	SPIF	SPIFH	DSIF	w
CUT	1	1/7	1/5	1/7	0.0328
ASPIF	7	1	5	1/3	0.3520
ASPIFH	5	1/5	1	7	0.3199
DSPIF	7	3	1/7	1	0.2953

**Table 8.** Comparison of the processing strategies with regards to C5 (energy consumption).

C5	CUT	SPIF	SPIFH	DSIF	w
CUT	1	3	5	5	0.4941
ASPIF	1/3	1	9	7	0.3713
ASPIFH	1/9	1/5	1	1/2	0.0528
DSPIF	1/7	1/5	2	1	0.0818

**Table 9.** Comparison of the processing strategies with regards to C6 (accuracy).

C6	CUT	SPIF	SPIFH	DSIF	w
CUT	1	7	5	3	0.5761
ASPIF	1/7	1	1/2	1/3	0.0715
ASPIFH	1/5	2	1	1/3	0.1125
DSPIF	1/3	3	3	1	0.2399

**Table 10.** Comparison of the processing strategies with regards to C7 (production time).

C7	CUT	SPIF	SPIFH	DSIF	w
CUT	1	5	5	7	0.5430
ASPIF	1/5	1	3	5	0.2445
ASPIFH	1/5	1/3	1	3	0.0765
DSPIF	1/7	1/5	1/3	1	0.1360

The matrix C will be built using the results from Tables 4–10. The columns of matrix C represent the eigenvectors resulting by comparing the four processes pairwise. The order of the columns within matrix C takes into consideration the order of the criteria determined in Table 2: C2, C1, C4, C6, C3, C7, and C5. Performing the multiplication of matrix C and the vector w, the preference vector x for the four manufacturing strategies may be obtained, according to the following relation:

$$x = Cw = \begin{bmatrix} 0.0399 & 0.1386 & 0.0328 & 0.5761 & 0.5143 & 0.5967 & 0.4941 \\ 0.6440 & 0.1622 & 0.3520 & 0.0715 & 0.3045 & 0.2292 & 0.3713 \\ 0.1145 & 0.2902 & 0.3199 & 0.1125 & 0.1158 & 0.0188 & 0.0528 \\ 0.2016 & 0.4090 & 0.2953 & 0.2399 & 0.0654 & 0.0553 & 0.0818 \end{bmatrix} \times \begin{bmatrix} 0.2256 \\ 0.3905 \\ 0.0558 \\ 0.1777 \\ 0.0233 \\ 0.0829 \\ 0.0442 \end{bmatrix} = \begin{bmatrix} 0.2506 \\ 0.2835 \\ 0.1919 \\ 0.2740 \end{bmatrix} \quad (6)$$

As can be noticed from Equation (6), the resulting column matrix has the highest value on the second line, 0.2835, a position which corresponds to the second analyzed manufacturing strategy, (ASPIF). According to this result, the AHP process has returned ASPIF as the most recommended approach if the seven proposed criteria are considered. Consequently, the experimental program was oriented to this process as the preferred solution for manufacturing cranioplasty plates. To assess the robustness and the reliability of the AHP process results, a sensitivity analysis was introduced according to the method proposed in [52,53]. According to this, the weights were changed while maintaining the ranking order previously determined. According to the proposed method, a coefficient  $\alpha \geq 0$  is introduced and the matrix A is transformed into  $[a_{ij}^\alpha]$ . If  $\alpha > 1$ , more dispersed weights are obtained and if  $\alpha < 1$ , the weights become more concentrated, without any change in the ranking order.

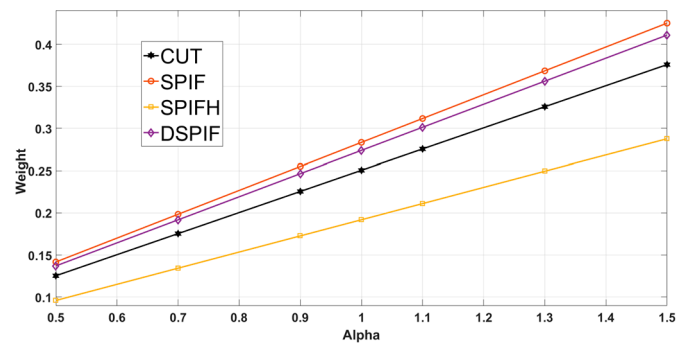
Table 11 shows the weights obtained for  $\alpha = 0.5, 0.7, 0.9, 1.0, 1.1, 1.3, 1.5$  (values proposed in [52]). Table 12 presents the simulation results of calculating the preference vector x for the weights from Table 11. A graphical synthesis of the sensitivity analysis is presented in Figure 3. It can be noticed that the changes in the weights do not affect the hierarchy of the preference vectors x; consequently, SPIF is the most recommended process for the entire range of the analysis.

**Table 11.** Sensitivity analysis for the weights.

Criterion	Coefficient $\alpha$						
	0.5	0.7	0.9	1.0	1.1	1.3	1.5
C1	0.1128	0.15792	0.20304	0.2256	0.24816	0.29328	0.3384
C2	0.19525	0.27335	0.35145	0.3905	0.42955	0.50765	0.58575
C3	0.0279	0.03906	0.05022	0.0558	0.06138	0.07254	0.0837
C4	0.08885	0.12439	0.15993	0.1777	0.19547	0.23101	0.26655
C5	0.01165	0.01631	0.02097	0.0233	0.02563	0.03029	0.03495
C6	0.04145	0.05803	0.07461	0.0829	0.09119	0.10777	0.12435
C7	0.0221	0.03094	0.03978	0.0442	0.04862	0.05746	0.0663

**Table 12.** Results of the sensitivity analysis simulations for the preference vector  $x$ .

Strategy	Coefficient $\alpha$ /Preference Vector $x$						
	0.5	0.7	0.9	1.0	1.1	1.3	1.5
CUT	0.1253	0.1754	0.2255	0.2506	0.2757	0.3258	0.3759
SPIF	0.1417	0.1984	0.2551	0.2835	0.3118	0.3685	0.4252
SPIFH	0.0959	0.1343	0.1727	0.1919	0.2111	0.2495	0.2878
DSPIF	0.1370	0.1918	0.2466	0.2740	0.3014	0.3562	0.4110

**Figure 3.** Graphical synthesis of the sensitivity analysis.

## 2.2. Experimental Layout

As stated in the literature review, one of the most used types of technological equipment for SPIF processing are CNC milling machines. For this research, a Haas MiniMill CNC machining center was used. The milling machine and the experimental layout mounted on the machine are presented in Figure 4.

**Figure 4.** Technological equipment: (a) Haas MiniMill computer numerically controlled (CNC) machining center; (b) Forming equipment (active die and retaining plate).

Figure 5 presents a 3D model of the forming equipment, where 1, punch; 2, active die; 3, retaining plate; 4, active die support; 5, baseplate; 6, fixing screws; 7, centering screw; and 8, sheet metal workpiece.

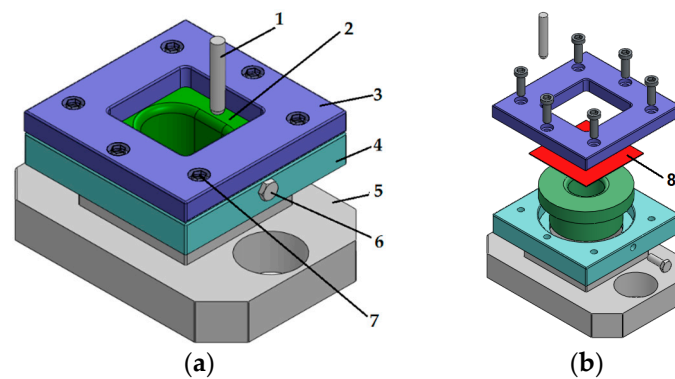


**Figure 5.** Forming equipment: (a) 3D model of the forming assembly—without the sheet metal workpiece; (b) Exploded view—with the sheet metal workpiece.

The active plate used for processing the parts is presented in Figure 6. Both the active die and the punch were made from 20Cr115 SR EN ISO 4957:2002 alloyed steel, heat treated.



**Figure 6.** Active die used for manufacturing the test parts.

### 2.3. Material

The chemical composition of Ti6Al4V titanium alloy in mass percentage is shown in Table 13.

Titanium is an allotropic substance consisting of a cubic structure ( $\alpha$ -Ti) and a compact hexagonal structure up to a temperature of 882 °C ( $\beta$ -Ti). As can be seen in Table 13, the main alloying elements are aluminum and vanadium, but besides these there are also other minor alloying elements such as iron, oxygen, nitrogen, hydrogen, silicon, and so on.

**Table 13.** Alloying elements of the Ti6Al4V material.

Alloy Element	Chemical Symbol	Mass Percentage (%)
Aluminum	Al	5.5–6.75
Vanadium	V	3.5–4.5
Carbon	C	0.10
Iron	Fe	0.3
Oxygen	O	0.02
Nitrogen	N	0.05
Hydrogen	H	0.015
Silicon	Si	0.15
Remainder	-	0.4

The mechanical characteristics of the titanium alloy Ti6Al4V are given in Table 14.

**Table 14.** Mechanical characteristics of the titanium alloy Ti6Al4V.

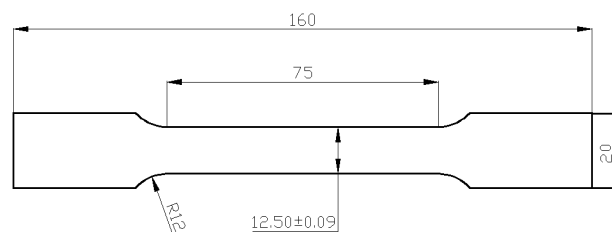
Characteristic	Measurement Unit	Value
Yield Strength	[MPa]	965–1103
Tensile Strength	[MPa]	896–1034
Density	[g/cm <sup>3</sup> ]	4.5
Modulus of Elasticity (Young modulus)	[GPa]	116

To determine the other mechanical characteristics of the material needed for finite element method (FEM) analysis, the tensile test was used. The tests were carried out for Ti6Al4V titanium alloy with a thickness of 0.5 mm, using the following laboratory equipment:

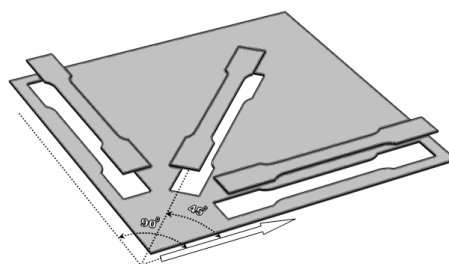
- tensile testing machine Instron 5587;
- optical strain measurement system GOM Aramis.

One of the methods of testing the deformation is the uniaxial traction test. On this machine, the specimen is fixed at both ends and deformed at a constant speed until cracking occurs.

Test specimens used for tensile testing are specimens with a calibrated length of 75 mm, a width of 12.5 mm, and a rectangular cross section (Figure 7) in accordance with the standard for the traction testing of metallic materials, SR EN 10002-1: 2002.

**Figure 7.** Specimens used for tensile testing.

To study the material anisotropy, sets of specimens were cut (by waterjet cutting) at 0°, 45°, and 90° angles to the sheet rolling direction; these are shown in Figure 8.

**Figure 8.** The different angles of the specimens.

The parameters related to the intrinsic properties of the material measured by traction test are hardening coefficient, coefficient of resistance, and coefficients of plastic anisotropy. The values will be used to define the elastoplastic behavior of the material in the FEM simulation. The tensile tests were performed on 3 sets of samples at room temperature, according to Table 15.

**Table 15.** Tensile tests.

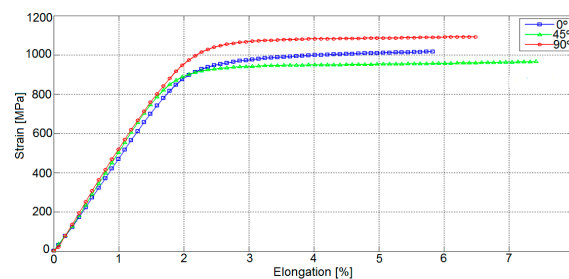
No.	No. of Specimens/Set	Direction of Lamination (°)	Temperature (°C)
1.	3	90°	25 °C
2.	3	0°	25 °C
3.	3	45°	25 °C

Using the BlueHill version 2.0 software (produced by Instron company, Norwood, MA, USA) to control the Instron 5587 Traction Testing Machine (produced also by Instron company), the following were set as input data: type of test, initial dimensions of the specimen, and deformation speed. Both BlueHill software and Instron machine are in the laboratories of Lucian Blaga University of Sibiu.

Following the data processing, the conventional strain curves ( $\sigma$ ) versus elongation ( $\varepsilon_{max}$ ) were obtained for the titanium alloy Ti6Al4V at room temperature, which are shown in Figure 9.

The mechanical characteristics of the material that were determined by the traction test are

- modulus of elasticity E [MPa],
- flow limit  $R_{p0.2}$  [MPa],
- tensile strength  $R_m$  [MPa],
- hardening coefficient n [-],
- resistance coefficient K [Pa],
- elongation  $\varepsilon_{max}$  [%].

**Figure 9.** Conventional strain curves ( $\sigma$ ) versus elongation ( $\varepsilon_{max}$ ).

In Table 16, a synthesis of the data obtained for the tensile testing for the three types of samples is presented.

**Table 16.** Synthesis of the data obtained from tensile tests.

Characteristic	Measurement Unit	Value		
Specimen Cutting Angle	[°]	0	45	90
The modulus of elasticity E	[MPa]	49,645.24	49,779.71	52,587.8
Flow Limit $R_{p0.2}$	[MPa]	881.9	863.11	922.51
Tensile Strength $R_m$	[MPa]	960.76	992.76	1001.35
Coefficient of hardening n	[-]	0.16	0.1	0.13
Resistance coefficient K	[Pa]	1618.9	1190.88	1392.81
Elongation $\varepsilon_{max}$	[%]	5.5	7.8	6.4

#### 2.4. Shape of Test Parts

To test the proposed technological approach, a truncated cone shape of the part was chosen. The geometry of the test part was defined by the cone angle ( $\alpha^\circ$ ), the height of the part ( $h$ ), and the diameter of the upper base ( $d$ ). The shape and dimensions of the parts are presented in Figure 10.

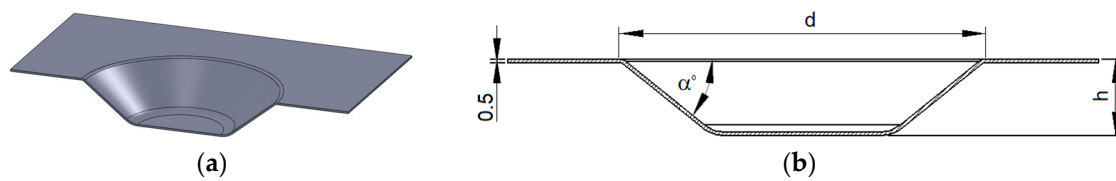


Figure 10. Test parts: (a) 3D model; (b) Characteristic dimensions.

### 2.5. Processing Trajectories

The processing trajectories were selected by taking into consideration the third objective stated above. According to the literature review, two main solutions have been imposed lately:

- contour-curves-based trajectory (a contour curve is obtained by intersecting the 3D shape by an XY plane—for the truncated cone, the contour curve is a circle);
- spatial spiral trajectory.

The trajectories used during the experimental test are synthesized in Table 17 and Figure 11.

Table 17. Trajectories.

Trajectory Type	Geometrical Primitive	Code	Observations
Circular trajectories	Contour curve (circle)	CT	The lead-in/lead-out points are lying on the same line (cone generatrix)
Circular trajectories with special entry points	Contour curve (circle)	CTSEP	The lead-in/lead-out points are distributed on the part surface
Spiral trajectories	Spatial spiral	ST	Only one lead-in and one lead-out point

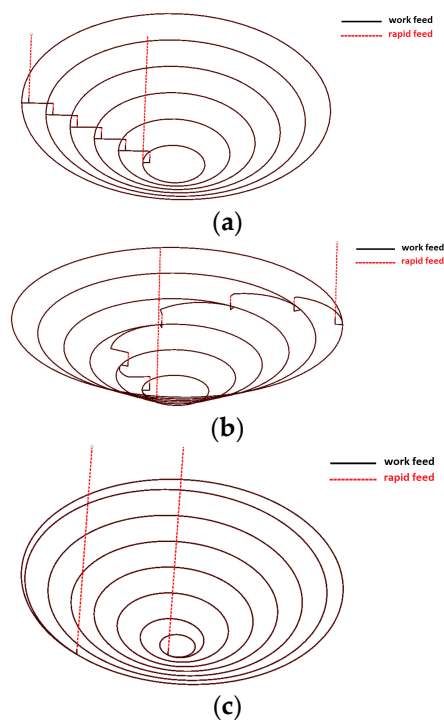
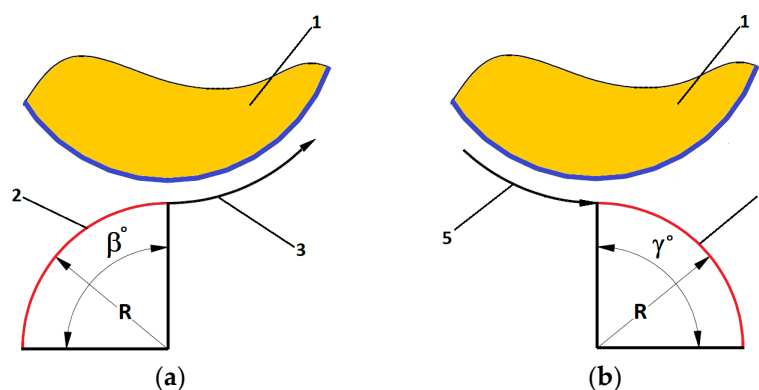


Figure 11. Processing trajectories: (a) Circular trajectories with the lead-in/lead-out points lying on the same line; (b) Circular trajectories with the lead-in/lead-out points distributed on the surface; (c) Spiral trajectories with only one lead-in and one lead-out point.

A computer-aided manufacturing software package, SprutCAM v. 11 (produced by Sprut Technology Ltd., Naberezhnye Chelny, Russia) dedicated for milling operations, was used for generating the trajectories. By using a commercially available CAM solution, the goal regarding ease of generation has been reached.

The circular trajectories (CT) (Figure 11a) have the drawback that all the lead-in points are situated on the same line, a cone generatrix. Lead-in points are the points where the tool (punch) enters in contact with the part. For the circular trajectories, the punch approaches the part with rapid feed, changes it in work feed in the near vicinity of the part, and enters in contact with the workpiece, all these movements being unfolded on the Z axis. After that, the relative movement between the punch and workpiece is unfolded in the XY plane, until a full circle is completed. After completing the circle, the punch performs a new lead-in movement combined on the XY plane and Z axis, and engages the part on a new circle, situated at distance  $p$  from the first one, where  $p$  is the vertical step of the SPIF process. In Figure 11a, all the lead-in points are situated on the same line, a situation which can lead to stress accumulation and, finally, to cracks. It is here noticeable that for a CAM solution for milling, aligning the lead-in points is a default procedure.

To avoid this drawback, the second approach was used. In the circular trajectories with special entry points (CTSEP) situation (Figure 11b), the lead-in points were distributed on the lateral surface of the truncated cone. To achieve this distribution, approach and retraction paths in the XY plane had to be defined (Figure 12) where 1, workpiece; 2, approach path in the XY plane; 3, start of the contour curve (circle); 4, retraction path in the XY plane; and 5, finish of the contour curve (circle).



**Figure 12.** Approach and retraction: (a) Approach path in the XY plane defined by radius  $R$  and angle  $\beta$ ; (b) Retraction path in the XY plane defined by radius  $R$  and angle  $\gamma$ .

The following relations for the values  $R$ ,  $\beta$ , and  $\gamma$  were used:

$$\beta = \gamma = 45^\circ \quad (6)$$

By combining the approach and retraction paths in the XY plane with the approach and retraction paths on the Z axis, the movement cycle of the punch may be divided as follows (Figure 13):

- the punch approaches on the Z axis with rapid feed (a);
- the punch continues the approach on the Z axis with work feed, until it reaches the contour curve level (b);
- the punch follows the approach path, in an XY plane at the Z level of the contour curve, until it is positioned on the contour curve (c);
- the punch follows the contour curve (d);
- the punch follows the retraction path, in the XY plane situated at the Z level of the contour curve (e);
- the punch approaches on the Z axis with rapid feed, travelling to the next contour curve (f);

- the punch continues the approach on the Z axis with work feed, until it reaches the next contour curve level—a new XY plane (g);
- after phase (g), the movements are repeating in a cycle, from d to g, until the last contour curve is processed.

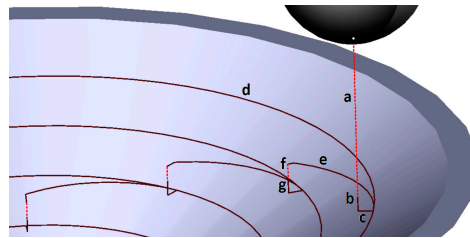


**Figure 13.** Movement phases for circular trajectories with special entry points (CTSEP).

By performing the movement phases described in Figure 12, the lead-in and lead-out points are distributed on the lateral surface of the cone, thus avoiding the accumulation of stresses and consequently avoiding the occurrence of cracks.

The third approach uses a spatial spiral trajectory (Figure 11c). In this case the trajectory is a continuous one, with only one entry point (lead-in) and one exit point (lead-out).

## 2.6. Processed Parts

The experimental tests were conducted according to the following parameters:

- The working feedrate was fixed to 150 mm/min;
- The punch was fixed in the main spindle of the machine and driven with a rotational speed of 150 rev/min around its own axis. According to the literature review, this rotation reduces the friction and has a favorable influence upon the formability of the material. However, the rotational speed was limited to avoid the heating of the material, which could affect its formability. The temperature limit in this case is 400 °C. At 150 rev/min, the temperature (measured during the process with an FLIR ThermoVision A320 thermal imaging camera (manufactured by FLIR Systems, Inc., Wilsonville, OR, USA) was found to be lower than 100 °C;
- The starting angle of the truncated cone was set to 30°, the next one was 35°, and afterwards the angle was incremented by 1°;
- Three vertical steps were considered: 0.2, 0.4, and 0.6 mm. Smaller steps, i.e., 0.1 mm were considered too small to be considered from a technological point of view, while steps greater than 0.6 mm lead to crack occurrence events at an angle of 30°;
- Two punch diameters were considered: 8 and 10 mm;
- Mineral oil was used as lubricant;
- At each angle, the first approach involved the use of the simplest trajectory (CT). If for a given angle this trajectory failed (crack occurrence), the CTSE was used instead. If the latter failed also, the ST trajectory was considered;
- The experimental tests are synthesized in Table 18. The lines in Table 18 only present the parts which were processed without cracks (successful tests). Each successful test was confirmed by performing it three times.

Table 18. Synthesis of the experimental tests.

Crt. No.	Base Diameter $d$ [mm]	Vertical Step $p$ [mm]	Height $h$ [mm]	Cone Angle $\alpha$ [°]	Punch Diameter $d_p$ [mm]	Trajectory Type
1.		0.4		30	8	CT
2.		0.4		30	10	CT
3.		0.6		30	8	CT
4.		0.6		30	10	CT
5.		0.2		35	8	CT
6.		0.2		35	10	CT
7.		0.4		35	8	CTSEP
8.		0.4		35	10	CTSEP
9.		0.6		35	8	CTSEP
10.		0.6		35	10	CTSEP
11.		0.2		36	8	CT
12.	55	0.2	12	36	10	CT
13.		0.4		36	8	CTSEP
14.		0.4		36	10	CTSEP
15.		0.6		36	8	ST
16.		0.6		36	10	CTSEP
17.		0.2		37	8	CTSEP
18.		0.2		37	10	CTSEP
19.		0.4		37	8	ST
20.		0.4		37	10	ST
21.		0.6		37	10	ST
22.		0.2		38	8	ST
23.		0.2		38	10	ST
24.		0.4		38	10	ST

Some of the successful tests are presented in Figures 14–16.

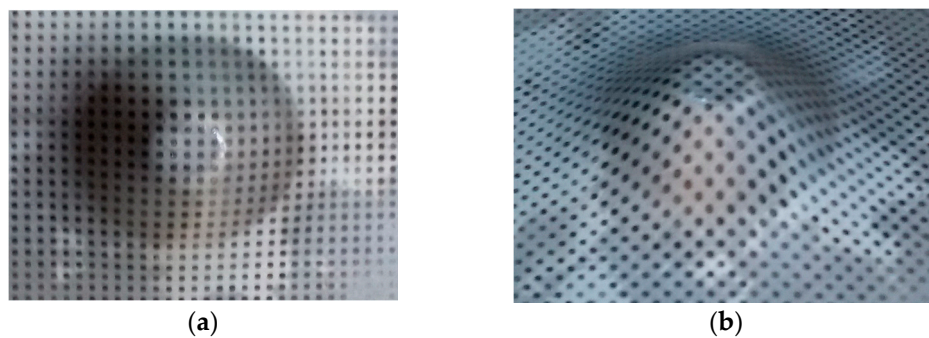


Figure 14. Part with  $p = 0.2$  mm,  $\alpha = 30^\circ$ ,  $d_p = 8$  mm, and CT. (a) view from above; (b) side view.

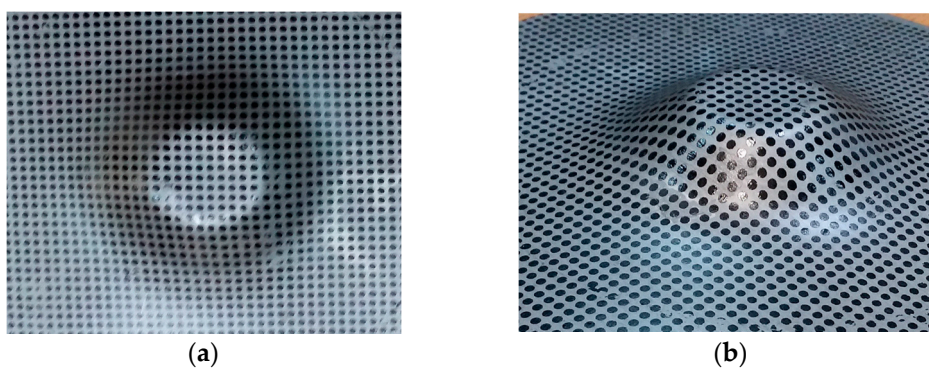
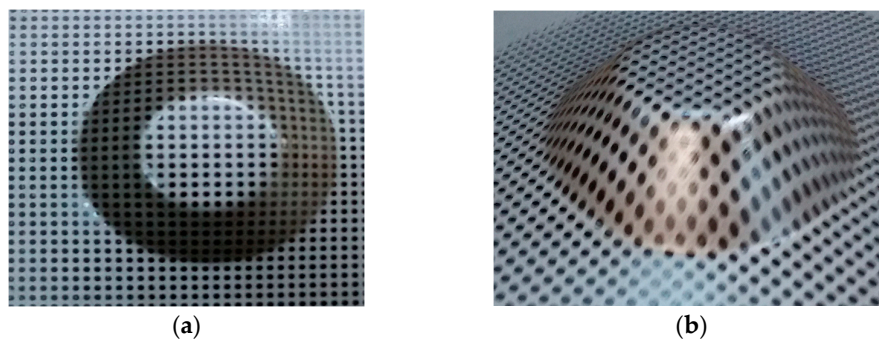
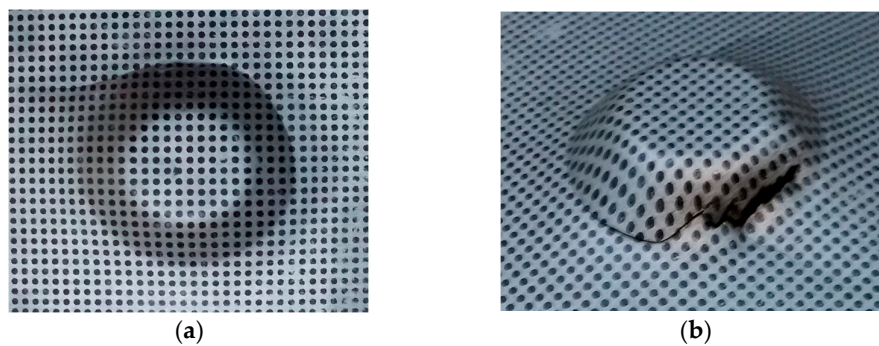


Figure 15. Part with  $p = 0.6$  mm,  $\alpha = 35^\circ$ ,  $d_p = 10$  mm, and CTSEP. (a) view form above; (b) side view.



**Figure 16.** Part with  $p = 0.4$  mm,  $\alpha = 38^\circ$ ,  $d_p = 10$  mm, and ST. (a) view from above; (b) side view.

Some examples of processed parts which cracked during the ASPIF process are presented in Figures 17–19.



**Figure 17.** Part with  $p = 0.6$  mm,  $\alpha = 35^\circ$ ,  $d_p = 8$  mm, and CT. (a) view from above; (b) side view.

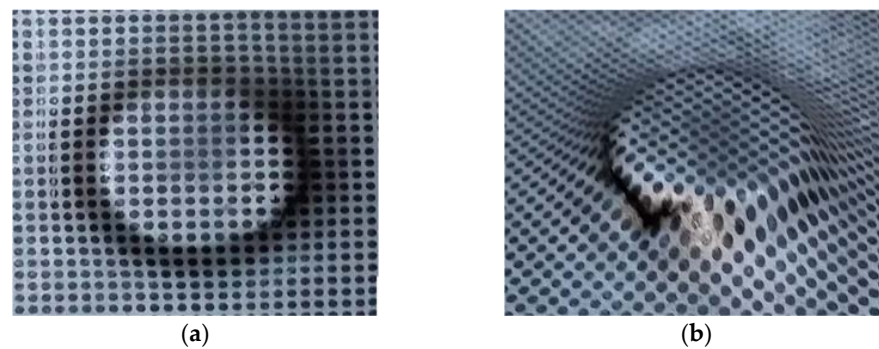


**Figure 18.** Part with  $p = 0.4$  mm,  $\alpha = 38^\circ$ ,  $d_p = 8$  mm, and ST. (a) view from above; (b) side view.

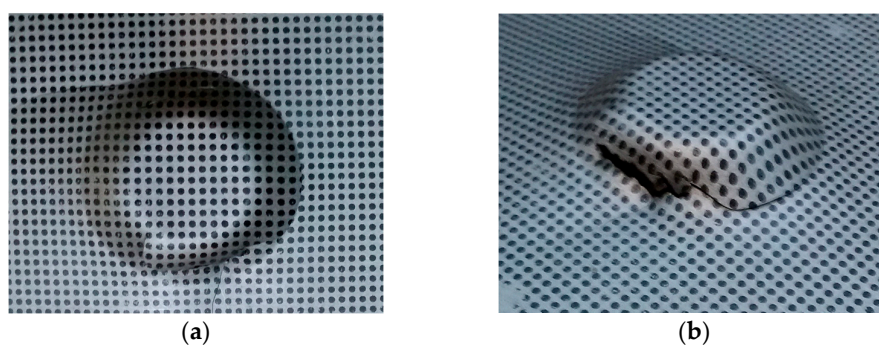


**Figure 19.** Part with  $p = 0.4$  mm,  $\alpha = 40^\circ$ ,  $d_p = 10$  mm, and ST. (a) view from above; (b) side view.

To test the accuracy of the processed parts, some measurements were performed using a Mahr profilometer (from Mahr GmbH, Göttingen, Germany). Figure 20 presents a graphical display of the measurement results for Part 24, while Table 19 presents a synthesis of the results for the measured parts. Even if more dimensional characteristics were measured, the results were focused on the angle  $\alpha^\circ$  and on the surface roughness (expressed by Ra and Rz). It is here noticeable the fact that taking into consideration the functional role intended for the parts (cranioplasty plates), their requested accuracy lies in a very different range compared with parts from the manufacturing industry, for example.

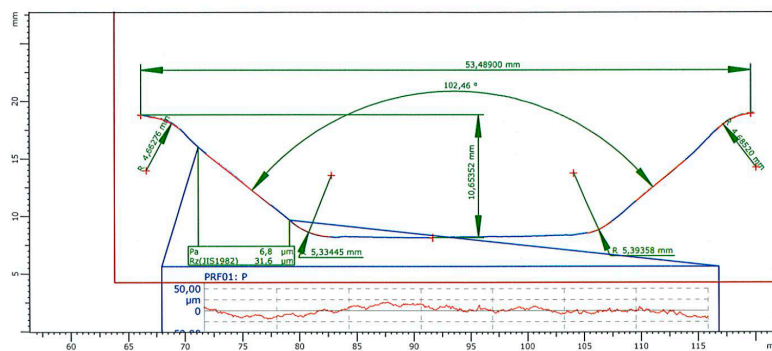


Figure 20. Measurement results for Part 24.

Table 19. Synthesis of results for the measured parts.

Part No.	Characteristics	Measured Values
1.	$\alpha^\circ = 30/p = 0.4/d_p = 8 \text{ mm}/\text{CT}$	$\alpha^\circ = 31.485$ Ra = 15.4 $\mu\text{m}$ /Rz = 23.1 $\mu\text{m}$
3.	$\alpha^\circ = 30/p = 0.6 \text{ mm}/d_p = 8 \text{ mm}/\text{CT}$	$\alpha^\circ = 31.125$ Ra = 19 $\mu\text{m}$ /Rz = 52.4 $\mu\text{m}$
6.	$\alpha^\circ = 35/p = 0.2 \text{ mm}/d_p = 10 \text{ mm}/\text{CT}$	$\alpha^\circ = 36.125$ Ra = 6 $\mu\text{m}$ /Rz = 35.3 $\mu\text{m}$
8.	$\alpha^\circ = 35/p = 0.4 \text{ mm}/d_p = 10 \text{ mm}/\text{CTSEP}$	$\alpha^\circ = 35.86$ Ra = 16.5 $\mu\text{m}$ /Rz = 58.2 $\mu\text{m}$
11.	$\alpha^\circ = 36/p = 0.2 \text{ mm}/d_p = 8 \text{ mm}/\text{CT}$	$\alpha^\circ = 35.865$ Ra = 10.3 $\mu\text{m}$ /Rz = 37.5 $\mu\text{m}$
18.	$\alpha^\circ = 37/p = 0.2 \text{ mm}/d_p = 10 \text{ mm}/\text{CTSEP}$	$\alpha^\circ = 38.8$ Ra = 8.3 $\mu\text{m}$ /Rz = 21 $\mu\text{m}$
23.	$\alpha^\circ = 38/p = 0.2 \text{ mm}/d_p = 10 \text{ mm}/\text{ST}$	$\alpha^\circ = 38.56$ Ra = 3.5 $\mu\text{m}$ /Rz = 18.3 $\mu\text{m}$
24.	$\alpha^\circ = 38/p = 0.4 \text{ mm}/d_p = 10 \text{ mm}/\text{ST}$	$\alpha^\circ = 38.77$ Ra = 6.8 $\mu\text{m}$ /Rz = 31.6 $\mu\text{m}$

### 2.7. FEM Analysis

The Abaqus/Explicit software package, v.14 (produced by Dassault Systèmes®, Vélizy-Villacoublay, France) as used for the FEM analysis. A parameterized model based upon the play between the punch and the active plate, the retention pressure, the diameter of the blank, and the radius of the active plate was developed. The geometric model included the sheet metal workpiece (considered as a deformable body), the active plate, the retention plate, and the punch (all being considered as rigid bodies). For the finite element mesh, four-node shell elements were used. The modeling was done on medium fiber, with five integration points per thickness being considered. The FEM model is presented in Figure 21.

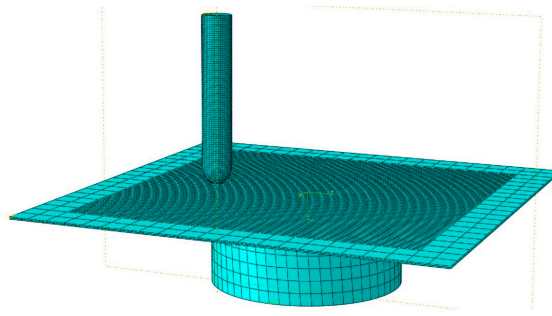


Figure 21. FEM model.

The parameters targeted by the FEM simulations were:

- major strains ( $\varepsilon_1$ );
- minor strains ( $\varepsilon_2$ );
- thickness reduction ( $s_{max}$ );
- evolution of the forming force on Z axis.

Figures 22–24 present the variations in  $\varepsilon_1$ ,  $\varepsilon_2$ , and  $s_{max}$  for a truncated cone with diameter of the upper base  $d = 55$  mm, cone angle  $\alpha = 30^\circ$ , vertical step  $p = 0.4$  mm, punch diameter  $d_p = 10$  mm, and spatial spiral trajectories.

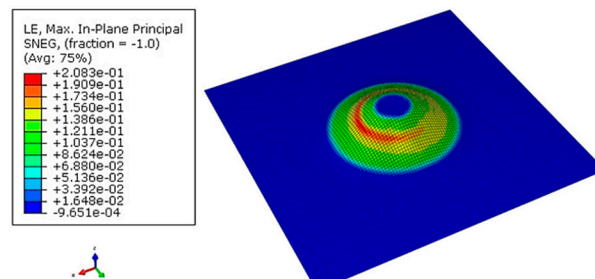


Figure 22. Distribution of major strains ( $\varepsilon_1$ )—diameter of the upper base  $d = 55$  mm, cone angle  $\alpha = 30^\circ$ , vertical step  $p = 0.4$  mm, punch diameter  $d_p = 10$  mm, and spatial spiral trajectories (ST).

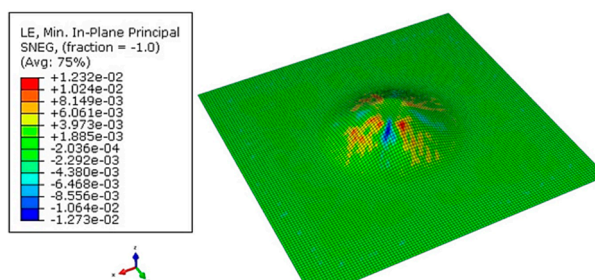
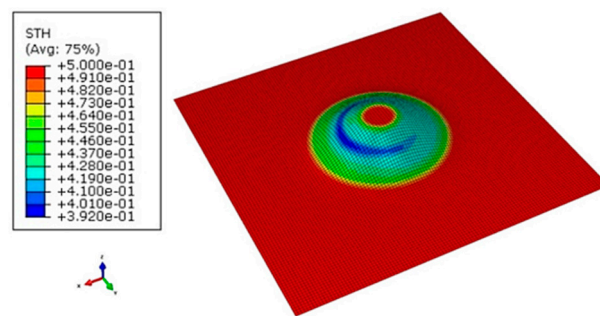
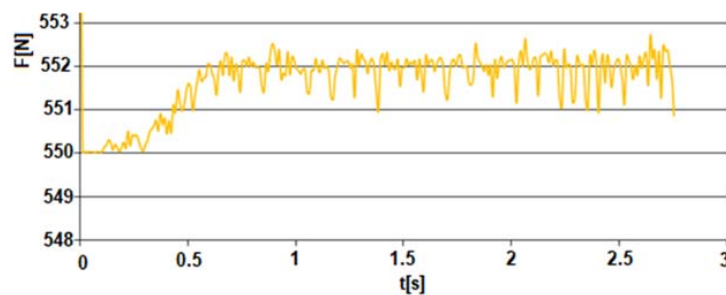


Figure 23. Distribution of minor strains ( $\varepsilon_2$ )—diameter of the upper base  $d = 55$  mm, cone angle  $\alpha = 30^\circ$ , vertical step  $p = 0.4$  mm, punch diameter  $d_p = 10$  mm, and spatial spiral trajectories (ST).



**Figure 24.** Thickness reduction ( $s_{max}$ )—diameter of the upper base  $d = 55$  mm, cone angle  $\alpha = 30^\circ$ , vertical step  $p = 0.4$  mm, punch diameter  $d_p = 10$  mm, and spatial spiral trajectories (ST).

Figures 25 and 26 present the simulated processing force on the Z axis, for the same part, diameter of the upper base  $d = 55$  mm, cone angle  $\alpha = 30^\circ$ , vertical step  $p = 0.4$  mm, and punch diameter  $d_p = 10$  mm, but for different types of trajectories—circles (Figure 22) and spatial spiral (Figure 23). It is here noticeable the fact that the simulation speed was increased by a magnification factor of 100; thus, the time scale covers the whole process.



**Figure 25.** Simulated processing forces on the Z axis—diameter of the upper base  $d = 55$  mm, cone angle  $\alpha = 30^\circ$ , vertical step  $p = 0.4$  mm, punch diameter  $d_p = 10$  mm, and circular trajectories (CT).

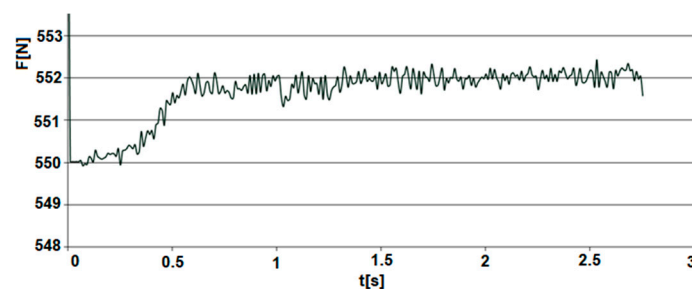


**Figure 26.** Simulated processing forces on the Z axis—diameter of the upper base  $d = 55$  mm, cone angle  $\alpha = 30^\circ$ , vertical step  $p = 0.4$  mm, punch diameter  $d_p = 10$  mm, and spatial spiral trajectories (ST).

A preliminary analysis reveals that the maximum values of the forces are quite similar, oscillating around 552 N. However, for the spiral trajectory, the amplitude of the oscillations is higher, a fact that could favor the occurrence of cracks.

## 2.8. Experimental Measurements

A GOM Argus optical system (produced by GOM company, Braunschweig, Germany) was used for measuring the parts. Figure 27 presents the experimental results for major strain ( $\epsilon_1$ ) distribution for the part with diameter of the upper base  $d = 55$  mm, cone angle  $\alpha = 30^\circ$ , vertical step  $p = 0.4$  mm, punch

diameter  $d_p = 8$  mm, and circular trajectories (CT). The maximum value of the major strain is 37.6%. Figure 28 presents the results for major strain ( $\epsilon_1$ ) distribution for the part with  $d = 55$  mm,  $\alpha = 35^\circ$ ,  $p = 0.4$  mm,  $d_p = 8$  mm, and circular trajectories with separate entry points (CTSE). The maximum value of the major strain is 34.1%. Figure 29 presents the results for major strain ( $\epsilon_1$ ) distribution for the part with  $d = 55$  mm,  $\alpha = 38^\circ$ ,  $p = 0.4$  mm,  $d_p = 10$  mm, and spatial spiral trajectories (ST). The maximum value of the major strain is 23.7%.

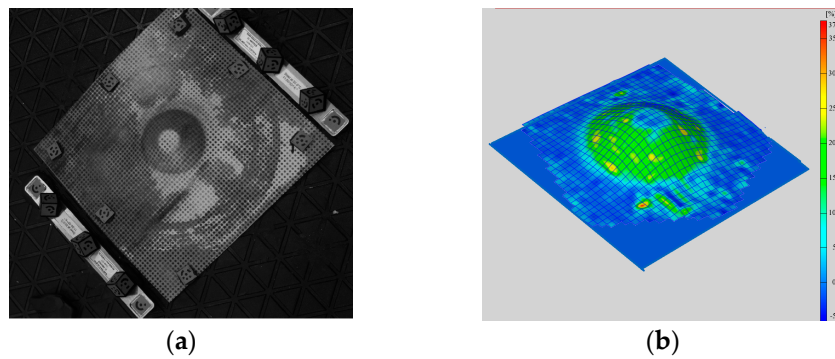


**Figure 27.** Measured distribution of major strains ( $\epsilon_1$ )—diameter of the upper base  $d = 55$  mm, cone angle  $\alpha = 30^\circ$ , vertical step  $p = 0.4$  mm, punch diameter  $d_p = 8$  mm, and circular trajectories (CT), (a) measured part; (b) measurement results.

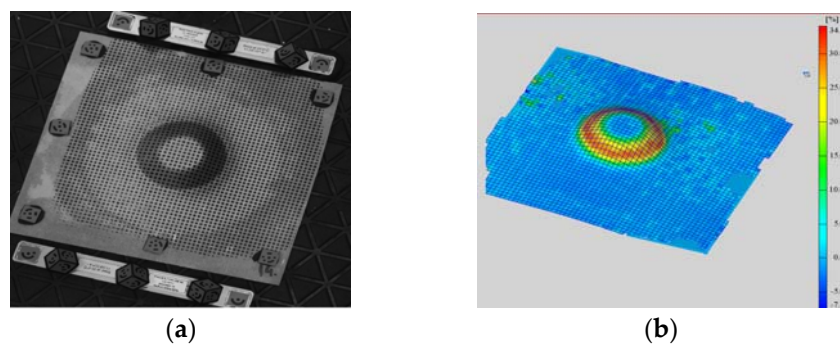


**Figure 28.** Measured distribution of major strains ( $\epsilon_1$ )—diameter of the upper base  $d = 55$  mm, cone angle  $\alpha = 35^\circ$ , vertical step  $p = 0.4$  mm, punch diameter  $d_p = 8$  mm, and circular trajectories with separate entry points (CTSEP), (a) measured part; (b) measured results.

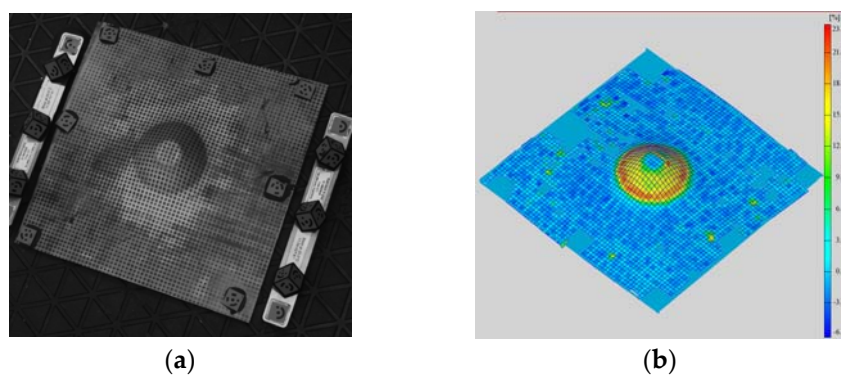


**Figure 29.** Measured distribution of major strains ( $\epsilon_1$ )—diameter of the upper base  $d = 55$  mm, cone angle  $\alpha = 38^\circ$ , vertical step  $p = 0.4$  mm, punch diameter  $d_p = 10$  mm, and spatial spiral trajectories (ST), (a) measured part; (b) measurement results.

A complete set of measured values of major strains ( $\epsilon_1$ ), minor strains ( $\epsilon_2$ ), and thickness reduction ( $s_{max}$ ) for the part with diameter of the upper base  $d = 55$  mm, cone angle  $\alpha = 30^\circ$ , vertical step  $p = 0.4$  mm, punch diameter  $d_p = 10$  mm, and spatial spiral trajectories (ST) is presented in Figure 30.

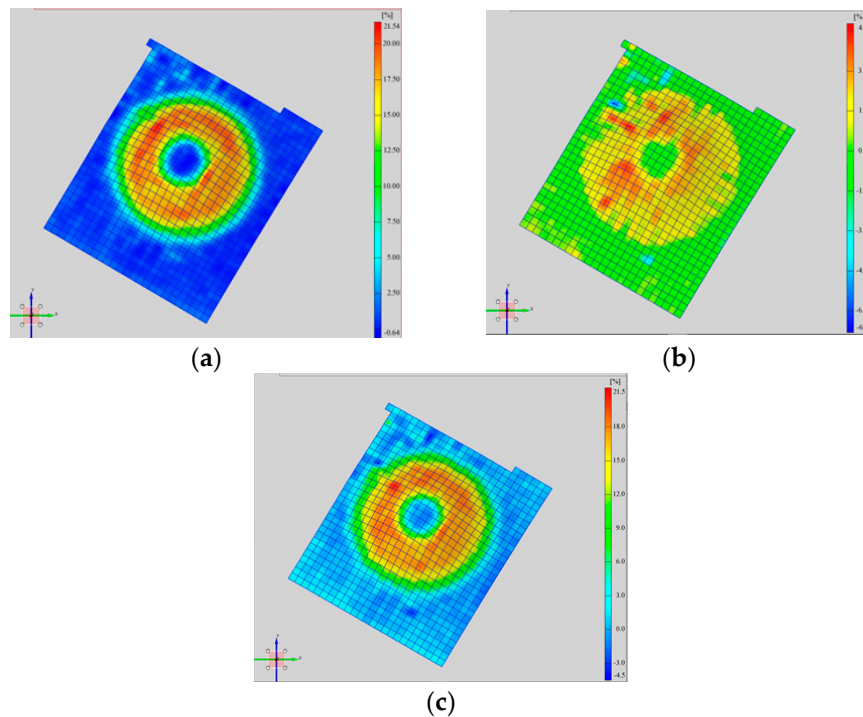


**Figure 30.** Measured values for major strains ( $\epsilon_1$ ) (a), minor strains ( $\epsilon_2$ ) (b), and thickness reduction ( $s_{max}$ ) (c) for the parts with diameter of the upper base  $d = 55$  mm, cone angle  $\alpha = 30^\circ$ , vertical step  $p = 0.4$  mm, punch diameter  $d_p = 10$  mm, and spatial spiral trajectories (ST).

A comparison between the simulated and the experimentally measured values for major strains ( $\epsilon_1$ ), minor strains ( $\epsilon_2$ ), and thickness reduction ( $s_{max}$ ) for the part with diameter of the upper base  $d = 55$  mm, cone angle  $\alpha = 30^\circ$ , vertical step  $p = 0.4$  mm, punch diameter  $d_p = 10$  mm, and spatial spiral trajectories (ST) is presented in Table 20.

**Table 20.** Comparison between simulated and measured values.

Part $d = 55$ mm, $\alpha = 30^\circ$ , $p = 0.4$ mm, $d_p = 10$ mm, ST	Characteristic Input					
	Major Strains $\epsilon_1$		Minor Strains $\epsilon_2$		Thickness Reduction $s_{max}$	
	%	log	%	log	%	log
Experimental	21.52	0.1951	4.78	0.0467	21.5	0.242
Simulated	-	0.2083	-	0.0123	-	0.216

### 2.9. Manufacturing a Cranioplasty Plate

The next step of the work was to process by means of SPIF a part with complex shape, specific for cranioplasty plates, to demonstrate that the proposed technological conditions allow the user to manufacture irregular shapes with rapid variations of the wall shapes and angles at room temperature. A manually made physical model was considered, taking into consideration the following requirements:

- The shape of the model had to be highly irregular, to mimic as close as possible the human skull;
- The shape of the model had to present rapid variations of the wall shapes and angles;

- Even if the experimental layout had size limitations, the overall area of the model was chosen about 40 cm<sup>2</sup> (exactly 36.5 cm<sup>2</sup>). According to the literature [54,55], this size could be considered as a quite common value for a cranial defect surface area.

After scanning the physical model, the 3D model of the part, presented in Figure 31, was stored in an stl file which resulted after processing a CT scan point cloud file.

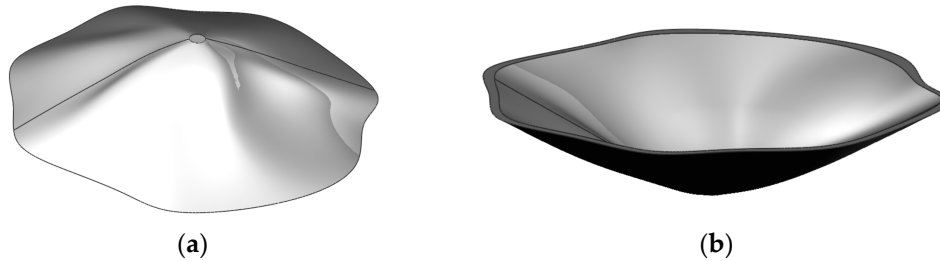


**Figure 31.** 3D model of the cranioplasty plate: (a) upper side; (b) lower side.

The shape of the plate is highly irregular and continuously variable, as can be seen from Figure 32. However, the wall angles were checked to be lower than 38° for any area of the part.

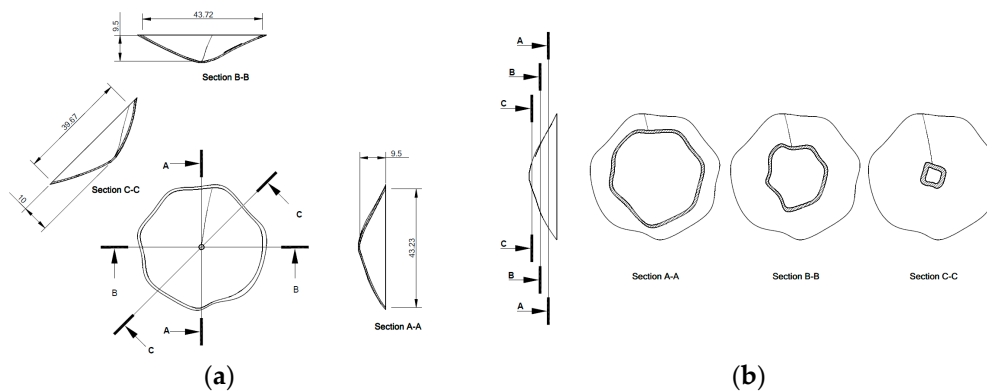


**Figure 32.** Geometry of the plate: (a) transversal sections; (b) horizontal sections.

Spatial spiral trajectories were used with a vertical step of  $p = 0.2$  mm and the punch with  $d_p = 10$  mm was chosen as the processing tool. Figure 33 presents the shape of the processing trajectories (toolpath), but for clarity, the vertical step was enlarged ten times (2 mm).

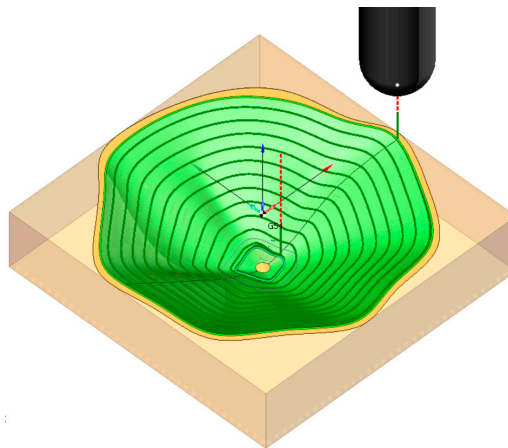


**Figure 33.** Spiral toolpath (for clarity of presentation, the vertical step was enlarged ten times).

The processed part is presented in Figure 34.

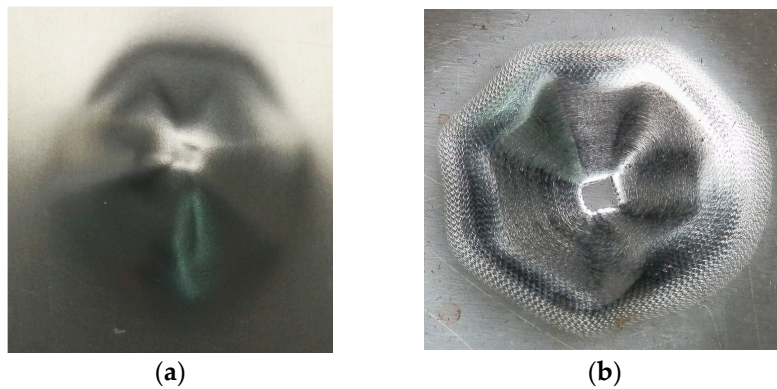


Figure 34. Processed part: (a) upper side; (b) lower side.

Using the Argus GOM optical measurement system, major strains ( $\epsilon_1$ ), minor strains ( $\epsilon_2$ ), and thickness reduction ( $s_{max}$ ) for the cranioplasty plates were measured. A synthesis of the values is presented in Table 21.

Table 21. Measured characteristic values for the cranioplasty plate.

Cranioplasty Plate	Characteristic Input		
	Major Strains $\epsilon_1$ [%]	Minor strains $\epsilon_2$ [%]	Thickness Reduction $s_{max}$ [%]
Characteristic	14.5	4.3	17.44

A graphical presentation of the measured values is presented in Figure 35.

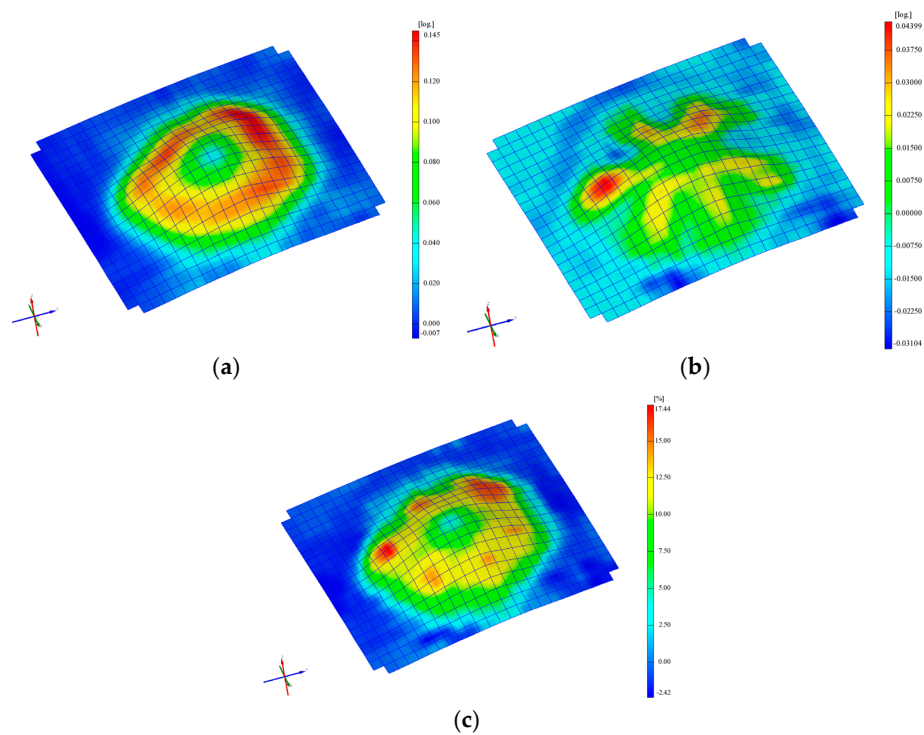


Figure 35. Measured values for major strains ( $\epsilon_1$ ) (a), minor strains ( $\epsilon_2$ ) (b), thickness reduction ( $s_{max}$ ) (c) for the cranioplasty plate.

From Table 21 and Figure 35, it can be noticed that the values of the characteristic inputs are in acceptable ranges for parts manufactured by means of SPIF. In fact, these values are even smaller than the ones obtained for the test parts (Table 20).

### 3. Results

The AHP method proposed here has indicated that SPIF is the most recommended manufacturing method if certain criteria are considered. Of course, the method could be affected by subjectivity, and the results could be changed if the analysis is done by other specialists. However, the performed sensitivity analysis guarantees, in some respects, the robustness of the results.

It is here noticeable that AHP indicates the best choice according to the criteria taken into consideration. Thus, if other sets of criteria are chosen, the results may differ significantly. The results presented in this work do not state that SPIF could be considered the best choice in any respect, but it could be considered the best choice if the criteria are those chosen in this approach.

An FEM model was developed which was able to provide simulation results close to values found experimentally for major and minor strains and for thickness reduction.

The experimental program provided some information regarding the technological conditions in which some incremental improvements (mainly an increase in the achievable wall angle) in the results of processing Ti6Al4V alloy at room temperature could be achieved. Also, it was presented that using continuous paths, a part with irregular shapes and with rapid variations of the wall shapes and angles has been processed.

Of course, there are also several shortcomings to this research:

- The processed test parts have limited dimensions (due to the available experimental layout), so it should be demonstrated by further study that the findings are also valid for bigger parts;
- Latest results presented in the literature [38,39] have indicated, by means of a cytotoxicity test, that heating the Ti6Al4V alloy during the SPIF process does not affect its biocompatibility. Corroborated by the superior plastic behavior of the heated material, these results narrow the application range of SPIF at room temperature. However, there are still reasons favoring the approach of SPIF at room temperature, from the points of view of roughness, costs (related to equipment complexity and energy consumption), and degree of control.

### 4. Conclusions

After conducting the experimental program, from a technological point of view it can be concluded that Ti6Al4V titanium alloy may be used for manufacturing cranioplasty plates, by processing by means of SPIF at room temperature, if the following technological aspects are considered:

- To reduce friction, the punch must rotate around its axis. A rotation speed between 150 and 300 rev/min was found during this experimental work to be appropriate;
- Theoretically, the working feed does not influence the formability of the part; however, it was found that working feeds greater than 200 mm/min may lead to crack occurrence. However, working feed affects the productivity, which is not critically important for this kind of part. Cranioplasty plates are manufactured as prototypes, productivity having less importance from this point of view;
- The vertical step of the punch (no matter if circular or spiral toolpaths are used) must be smaller than 1 mm. Best results were achieved by using vertical steps of 0.6, 0.4, and 0.2 mm. A direct link was noticed between the vertical step and the maximum inclination angle ( $\alpha^\circ$ ) of the wall: the smaller the vertical step, the larger the achievable angle;
- Continuous toolpaths (which do not use lead-in/lead out entry/exit points) are the best approach, because entry/exit points may become stress concentrators leading to crack occurrence. Spatial spiral trajectories provide the best results, but for irregular shapes, generating them without the aid of CAM software is difficult. Another solution is to use contour curves spaced on the Z axis as

trajectories (circles or another curves) and distribute the lead-in/lead out points on the surface of the part (avoiding placing them close to each other);

- The maximum achievable wall angle was found  $\alpha = 38^\circ$ ;
- The best results, from the point of view of both the accuracy and surface roughness, were obtained using the punch with diameter  $d_p = 10$  mm (compared with the punch with  $d_p = 8$  mm);
- The accuracy of the wall angle was not significantly influenced by the diameter of the punch or by the vertical step. Also, the toolpaths did not influence it. The explanation for this may be found in the fact that the low plasticity of the Ti6Al4V titanium alloy does not lead to significant values of the springback;
- The roughness of the parts was influenced by the vertical step directly, a decrease in the vertical step leading to a decrease in the roughness value.
- Further research will be oriented in the following directions:
- The influence of rotational speed and working feed upon the accuracy of the part will be studied in more detail;
- For the time being, the overall dimensions of the parts were limited by the size of the experimental layout (mainly the size of the active plate and the working space of the CNC machine-tool). A new layout will be designed and implemented to test how greater overall dimensions of the part influence its manufacturability by means of ASPIF at room temperature;
- Industrial robots will be used as technological equipment to test if superior kinematics (more complex processing trajectories) can improve the manufacturability of the parts.

**Author Contributions:** S.G.R., M.T. and O.B. designed and set up the experimental layouts and the experimental program, R.E.B. set up the machining strategies, performed the AHP analysis, and wrote the paper, S.G.R., C.G., C.B. and A.L.C. performed the formability measurements and data analysis.

**Funding:** This research was funded by the Romanian Ministry of Research and Innovation CCCDI-UEFISCDI, project number PN-III-P1-1.2-PCCDI-2017-0446/nr. 82PCCDI/2018, within PNCDI III, project title: "Intelligent manufacturing technologies for advanced production of parts".

**Conflicts of Interest:** The authors declare no conflict of interest.

## References

1. Rack, H.J.; Qazi, J.I. Titanium alloys for biomedical applications. *Mater. Sci. Eng. C* **2006**, *26*, 1269–1277. [[CrossRef](#)]
2. Geetha, M.; Singh, A.K.; Asokamani, R.; Gogia, A.K. Ti based biomaterials, the ultimate choice for orthopaedic implants—A review. *Prog. Mater. Sci.* **2009**, *54*, 397–425. [[CrossRef](#)]
3. Williams, D.F. On the mechanisms of biocompatibility. *Biomaterials* **2008**, *29*, 2941–2953. [[CrossRef](#)] [[PubMed](#)]
4. Aydin, S.; Kucukyuruk, B.; Abuzayed, B.; Aydin, S.; Sanus, G.Z. Cranioplasty: Review of materials and techniques. *J. Neurosci. Rural Pract.* **2011**, *2*, 162–167. [[PubMed](#)]
5. Servadei, F.; Iaccarino, C. The Therapeutic cranioplasty still needs an ideal material and surgical timing. *World Neurosurg.* **2015**, *83*, 133–135. [[CrossRef](#)] [[PubMed](#)]
6. Joffe, J.M.; Nicoll, S.R.; Richards, R.; Linney, A.D.; Harris, M. Validation of computer-assisted manufacture of titanium plates for cranioplasty. *Int. J. Oral Maxillofac. Surg.* **1999**, *28*, 309–313. [[CrossRef](#)]
7. Wiggins, A.; Austerberry, R.; Morrison, D.; Kwok, H.M.; Honeybul, S. Cranioplasty with custom-made titanium plates—14 years experience. *Neurosurgery* **2013**, *72*, 248–256. [[CrossRef](#)] [[PubMed](#)]
8. Heissler, E.; Fischer, F.-S.; Boiouri, S.; Lehrmann, T.; Mathar, W.; Gebhardt, A.; Lanksch, W.; Bler, J. Custom-made cast titanium implants produced with CAD/CAM for the reconstruction of cranium defects. *Int. J. Oral Maxillofac. Surg.* **1998**, *27*, 334–338. [[CrossRef](#)]
9. Cabraja, M.; Klein, M.; Lehmann, T.-N. Long-term results following titanium cranioplasty of large skull defects. *Neurosurg. Focus* **2009**, *26*, 1–7. [[CrossRef](#)] [[PubMed](#)]
10. Bhargava, D.; Bartlett, P.; Russell, J.; Liddington, M.; Tyagi, A.; Chumas, P. Construction of titanium cranioplasty plate using craniectomy bone flap as template. *Acta Neurochir.* **2010**, *152*, 173–176. [[CrossRef](#)] [[PubMed](#)]

11. Chen, J.-J.; Liu, W.; Li, M.-Z.; Wang, C.-T. Digital manufacture of titanium prosthesis for cranioplasty. *Int. J. Adv. Manuf. Technol.* **2006**, *27*, 1148–1152. [[CrossRef](#)]
12. Che-Haron, C.H.; Jawaid, A. The effect of machining on surface integrity of titanium alloy Ti–6% Al–4% V. *J. Mater. Process. Technol.* **2005**, *166*, 188–192. [[CrossRef](#)]
13. Jeswiet, J.; Micari, F.; Hirt, G.; Bramley, A.; Dufloy, J.; Allwood, J. Asymmetric single point incremental forming of sheet metal. *CIRP Ann. Manuf. Technol.* **2005**, *54*, 623–650. [[CrossRef](#)]
14. Behera, A.K.; de Sousa, R.A.; Ingarao, G.; Oleksik, V. Single point incremental forming: An assessment of the progress and technology trends from 2005 to 2015. *J. Manuf. Process.* **2017**, *27*, 37–62. [[CrossRef](#)]
15. Gatea, S.; Ou, H.; McCartney, G. Review on the influence of process parameters in incremental sheet forming. *Int. J. Adv. Manuf. Technol.* **2016**, *87*, 479–499. [[CrossRef](#)]
16. Hussain, G.; Gao, L.; Hayat, N.; Cui, Z.; Pang, Y.C.; Dar, N.U. Tool and lubrication for negative incremental forming of a commercially pure titanium sheet. *J. Mater. Process. Technol.* **2008**, *203*, 193–201. [[CrossRef](#)]
17. Hamilton, K.; Jeswiet, J. Single point incremental forming at high feed rates and rotational speeds: Surface and structural consequences. *CIRP Ann. Manuf. Technol.* **2010**, *59*, 311–314. [[CrossRef](#)]
18. Kim, Y.H.; Park, J.J. Effect of process parameters on formability in incremental forming of sheet metal. *J. Mater. Process. Technol.* **2002**, *130–131*, 42–46. [[CrossRef](#)]
19. Durante, M.; Formisano, A.; Langella, A.; Memola Capece Minutolo, F. The influence of tool rotation on an incremental forming process. *J. Mater. Process. Technol.* **2009**, *209*, 4621–4626. [[CrossRef](#)]
20. Ambrogio, G.; Gagliardi, F.; Bruschi, S.; Filice, L. On the high-speed Single Point Incremental Forming of titanium alloys. *CIRP Ann. Manuf. Technol.* **2013**, *62*, 243–246. [[CrossRef](#)]
21. Fan, G.; Gao, L.; Hussain, G.; Wu, Z. Electric hot incremental forming: A novel technique. *Int. J. Mach. Tools Manuf.* **2008**, *48*, 1688–1692. [[CrossRef](#)]
22. Ambrogio, G.; Filice, L.; Gagliardi, F. Formability of lightweight alloys by hot incremental sheet forming. *Mater. Des.* **2012**, *34*, 501–508. [[CrossRef](#)]
23. Palumbo, G.; Brandizzi, M. Experimental investigations on the single point incremental forming of a titanium alloy component combining static heating with high tool rotation speed. *Mater. Des.* **2012**, *40*, 43–51. [[CrossRef](#)]
24. Göttmann, A.; Diettrich, J.; Bergweiler, G.; Bambach, M.; Hirt, G.; Loosen, P.; Poprawe, R. Laser-assisted asymmetric incremental sheet forming of titanium sheet metal parts. *Prod. Eng.* **2011**, *5*, 263–271. [[CrossRef](#)]
25. Xu, D.; Wu, W.; Malhotra, R.; Chen, J.; Lu, B.; Cao, J. Mechanism investigation for the influence of tool rotation and laser surface texturing (LST) on formability in single point incremental forming. *Int. J. Mach. Tools Manuf.* **2013**, *73*, 37–46. [[CrossRef](#)]
26. Xu, D.K.; Lu, B.; Cao, T.T.; Zhang, H.; Chen, J.; Long, H.; Cao, J. Enhancement of process capabilities in electrically-assisted double sided incremental forming. *Mater. Des.* **2016**, *92*, 268–280. [[CrossRef](#)]
27. Feng, B.; Chen, J.Y.; Oi, S.K.; He, L.; Zhao, J.Z.; Zhang, X.D. Characterization of surface oxide films on titanium and bioactivity. *J. Mater. Sci. Mater. Med.* **2002**, *13*, 457–464.
28. Guleryuz, H.; Cimenoglu, H. Surface modification of a Ti–6Al–4V alloy by thermal oxidation. *Surf. Coat. Technol.* **2005**, *192*, 164–170. [[CrossRef](#)]
29. Duarte, L.T.; Bolfarini, C.; Biaggio, S.R.; Rocha-Filho, R.C.; Nascente, P.A.P. Growth of aluminum-free porous oxide layers on titanium and its alloys Ti–6Al–4V and Ti–6Al–7Nb by micro-arc oxidation. *Mater. Sci. Eng. C* **2014**, *41*, 343–348. [[CrossRef](#)] [[PubMed](#)]
30. Guleryuz, H.; Cimenoglu, H. Oxidation of Ti–6Al–4V alloy. *J. Alloys Compd.* **2009**, *472*, 241–246. [[CrossRef](#)]
31. Chen, M.; Li, W.; Shen, M.; Zhu, S.; Wang, F. Glass–ceramic coatings on titanium alloys for high temperature oxidation protection: Oxidation kinetics and microstructure. *Corros. Sci.* **2013**, *74*, 178–186. [[CrossRef](#)]
32. Zhang, Y.; Maa, G.-R.; Zhang, X.-C.; Li, S.; Tu, S.-T. Thermal oxidation of Ti–6Al–4V alloy and pure titanium under external bending strain: Experiment and modelling. *Corros. Sci.* **2017**, *122*, 61–73. [[CrossRef](#)]
33. Du, H.L.; Datta, P.K.; Lewis, D.B.; Burnell-Gray, J.S. Air oxidation behavior of Ti–6Al–4 V alloy between 650 and 850 °C. *Corros. Sci.* **1994**, *36*, 631–642. [[CrossRef](#)]
34. McLachlan, D.R.C. Aluminium and the risk for Alzheimer’s disease. *Environmetrics* **1995**, *6*, 233–275. [[CrossRef](#)]
35. Aniołek, K.; Kupka, M.; Barylski, A.; Dercz, G. Mechanical and tribological properties of oxide layers obtained on titanium in the thermal oxidation process. *Appl. Surf. Sci.* **2015**, *357*, 1419–1426. [[CrossRef](#)]

36. Luo, Y.; Chen, W.; Tian, M.; Teng, S. Thermal oxidation of Ti6Al4V alloy and its biotribological properties under serum lubrication. *Tribol. Int.* **2015**, *89*, 67–71. [[CrossRef](#)]
37. Aniolek, K. The influence of thermal oxidation parameters on the growth of oxide layers on titanium. *Vacuum* **2017**, *144*, 94–100. [[CrossRef](#)]
38. Ambrogio, G.; Sgambitterra, E.; De Napoli, L.; Gagliardi, F.; Fragomeni, G.; Piccininni, A.; Guglielmi, P.; Palumbo, G.; Sorgente, D.; La Barbera, L.; et al. Performances analysis of titanium prostheses manufactured by superplastic forming and incremental forming. *Procedia Eng.* **2017**, *183*, 168–173. [[CrossRef](#)]
39. Palumbo, G.; Sorgente, D.; Vedani, M.; Mostaed, E.; Hamidi, M.; Gastaldi, D.; Villa, T. Effects of superplastic forming on modification of surface properties of Ti alloys for biomedical applications. *J. Manuf. Sci. Eng.* **2018**, *140*, 10. [[CrossRef](#)]
40. Ingarao, G.; Ambrogio, G.; Gagliardi, F.; Di Lorenzo, R. A sustainability point of view on sheet metal forming operations: Material wasting and energy consumption in incremental forming and stamping processes. *J. Clean. Prod.* **2012**, 29–30, 255–268. [[CrossRef](#)]
41. Bagudanch, I.; Garcia-Romeu, M.L.; Ferrer, I.; Lupiañez, J. The effect of process parameters on the energy consumption in single point incremental forming. *Procedia Eng.* **2013**, *63*, 346–353. [[CrossRef](#)]
42. Ingarao, G.; Vanhove, H.; Kellens, K.; Duflou, J.R. A comprehensive analysis of electric energy consumption of single point incremental forming processes. *J. Clean. Prod.* **2014**, *67*, 173–186. [[CrossRef](#)]
43. Ambrogio, G.; Ingarao, G.; Gagliardi, F.; Di Lorenzo, R. Analysis of energy efficiency of different setups able to perform single point incremental forming (SPIF) Processes. *Procedia CIRP* **2014**, *15*, 111–116. [[CrossRef](#)]
44. Breaz, R.; Bologa, O.; Tera, M.; Racz, G. Researches Regarding the Use of Complex Trajectories and Two Stages Processing in Single Point Incremental Forming of Two Layers Sheet. *Circles* **2012**, *91*, 128.
45. Breaz, R.; Bologa, O.; Tera, M.; Racz, G. Computer assisted techniques for the incremental forming technology. In Proceedings of the IEEE 18th Conference on Emerging Technologies & Factory Automation (ETFA), Cagliari, Italy, 10–13 September 2013.
46. Cotigă, C.; Bologa, O.; Racz, S.G.; Breaz, R.E. Researches regarding the usage of titanium alloys in cranial implants. *Appl. Mech. Mater.* **2014**, *657*, 173–177. [[CrossRef](#)]
47. Kim, B.J.; Hong, K.S.; Park, K.J.; Park, D.H.; Chung, Y.G.; Kang, S.H. Customized cranioplasty implants using three-dimensional printers and polymethyl-methacrylate casting. *J. Korean Neurosurg. Soc.* **2012**, *52*, 541–546. [[CrossRef](#)] [[PubMed](#)]
48. Digital Evolution of Cranial Surgery. Available online: <http://www.renishaw.com/en/digital-evolution-of-cranial-surgery--38602> (accessed on 7 August 2018).
49. Saaty, T.L. *The Analytic Hierarchy Process: Planning, Priority Setting, Resource Allocation*; McGraw-Hill: New York, NY, USA, 1980; p. 287.
50. Saaty, T.L. *Decision Making for Leaders: The Analytic Hierarchy Process for Decisions in a Complex World*; RWS Publication: Pittsburgh, PA, USA, 1990.
51. Alonso, J.; Lamata, T.M. Consistency in the analytic hierarchy process: A new approach. *Int. J. Uncertain. Fuzziness Knowl. Based Syst.* **2006**, *14*, 445–459. [[CrossRef](#)]
52. Cabala, P. Using the analytic hierarchy process in evaluating decision alternatives. *Oper. Res. Decis.* **2010**, *20*, 5–23.
53. Hurley, W.J. The analytic hierarchy process: A note on an approach to sensitivity which preserves rank order. *Comput. Oper. Res.* **2001**, *28*, 185–188. [[CrossRef](#)]
54. Williams, L.R.; Fan, K.F.; Bentley, R.P. Custom-made titanium cranioplasty: Early and late complications of 151 cranioplasties and review of the literature. *Int. J. Oral Maxillofac. Surg.* **2015**, *44*, 599–608. [[CrossRef](#)] [[PubMed](#)]
55. Williams, L.; Fan, K.; Bentley, R. Titanium cranioplasty in children and adolescents. *J. Cranio Maxillofac. Surg.* **2016**, *44*, 789–794. [[CrossRef](#)] [[PubMed](#)]

